Virtual Impedance-based Phase Modifier for Fault Type Classification in IBR-Connected Lines

Sourav Maity
Department of Electrical Engineering
Indian Institute of Technology Indore
Indore, Madhya Pradesh, India
phd2301202010@iiti.ac.in

Ankit Kumar
Department of Electrical Engineering
Indian Institute of Technology Indore
Indore, Madhya Pradesh, India
ee220002009@iiti.ac.in

Subhadeep Paladhi
Department of Electrical Engineering
Indian Institute of Technology Indore
Indore, Madhya Pradesh, India
spaladhi@iiti.ac.in

***Abstract*—Fault ride through capability, a necessary mandate by the grid codes for large-scale inverter-based resources (IBR), prevent those from disconnection during faults in the networks. The converter control actions in such plants can substantially alter the network's fault signature, causing conventional fault type classifiers to maloperate at times. This work proposes a design of an adaptive virtual impedance-based phase modifier, which aligns the sequence currents obtained at relay bus with the faulted path currents. Thus, the phase angles associated with faulted path sequence currents, which always maintain a distinct relationship for different fault types, are reconstructed to identify fault type in IBR-connected lines. The technique is evaluated under a broad set of fault conditions on IBR-integrated 9-bus power system, modeled in PSCAD/EMTDC. Simulation results confirm that the proposed method maintains high classification accuracy across diverse fault conditions with various IBR technologies. Comparative analyses highlight its superior robustness and performance. A hardware prototype is developed incorporating the proposed fault type classification technique using Arduino UNO R4 Wi-Fi board interfaced with MATLAB and tested with the simulated data.**

***Index Terms*—Fault type classification, inverter-based resources, line protection, faulted phase selection.**

I. Introduction

GROWING environmental concerns have accelerated the large-scale deployment of inverter-based resources (IBRs) into high-voltage transmission networks [1]. To ensure reliable operation of power systems dominated by variable renewable generation such as solar and wind plants, converters associated with these resources employ various advanced control strategies. Grid codes further mandate fault ride-through (FRT) capability, requiring IBRs to remain connected even during network faults [2]. The inverter-driven control actions significantly influence the faulted voltage and current profiles, producing characteristics that differ from those of conventional synchronous generation. These altered signatures challenge existing protection schemes, making accurate fault type identification increasingly critical [3]–[5]. Fault type classification plays a vital role in several transmission-level protection functions, including single-pole tripping and distance protection [6]. Considering the diversity of IBR control techniques, varying grid code obligations, and system non-uniformity, there is a clear need to reassess and enhance current fault classification methodologies.

Existing fault classification methods are reviewed by segregating into four general categories.

A. Commercial relay algorithms

Conventional relays typically use phase-angle relationships of sequence currents and voltages to identify fault types, and they generally perform well in systems dominated by synchronous generators [7], [8]. Variants include using negative and zero sequence current angle differences or incorporating superimposed sequence voltages for weak-infeed conditions. However, these schemes assume system homogeneity and struggle in IBR-rich grids where converter controls alter fault signatures.

B. Data-driven approaches with/without signal processing

Machine-learning classifiers (like neural networks, fuzzy logic, decision trees, and hybrid techniques) have been applied for faulted phase selection using features extracted through tools like wavelet transforms or S-transforms [9], [10]. Their effectiveness is limited in IBR-dominated systems, where obtaining large training datasets with changing fault patterns due to converter-driven dynamics seems impractical.

C. Controller-Based Modifications

Some works propose modification in inverter controllers (e.g., dual-current control) so that IBRs replicate synchronous-generator fault behavior [11]. Such modifications, however, are difficult to generalize across diverse IBR technologies, and grid conditions.

D. Other Specialized Approaches

Waveform correlation–based time-domain techniques and some advanced classifiers have also been proposed, but those either require signals sampled at a very high rate or rely on assumption like small voltage angle differences between buses that do not hold for long transmission lines [12], [13]. System-wide PMU-based approaches face communication delays that make them unsuitable for fast protection [14].

In this work, a technique is proposed to design a virtual impedance-based phase modifier for correct identification of fault type in IBR-connected lines. Value of the virtual impedance is controlled by the local voltage and current

979-8-3315-8138-1

measurements during fault, and adaptive to the fault and system conditions. The phase modifier aligns the positive and negative sequence currents measured at the relay bus with the corresponding faulted path currents, which follows a distinct phase-relationship for each fault type. The proposed method is evaluated under diverse fault conditions, and in the presence of different IBRs on the standard 9-bus test system modeled in PSCAD/EMTDC. Its performance is found consistently high and accurate. Comparative studies confirm that the proposed method outperforms existing approaches. A hardware prototype is developed incorporating the proposed fault type classification technique using Arduino UNO R4 Wi-Fi board interfaced with MATLAB and tested with the simulated data obtained from PSCAD.

II. Proposed Fault Type Classification Technique

The proposed fault type classification technique is presented in this section in two steps. First, system-independent fault zones are identified by analyzing the sequence networks for different types of faults. Second step describes the design of an adaptive virtual impedance-based phase modifier to drive the local sequence currents to maintain the index following fault zones correctly.

A. Formulation of phase selection zones

A grid-following IBR is typically modeled as a dependent current source (I_{IBR}) in parallel with a variable impedance (Z_{IBR}) and can be transformed into an equivalent voltage source model, as illustrated in Fig. 1(a). This equivalent form may further be transformed to a fixed voltage source in series with a variable impedance, as shown in Fig. 1(b), where variations in the source are reflected as voltage drops across an added virtual impedance included within Z_{IBR}. A simplified

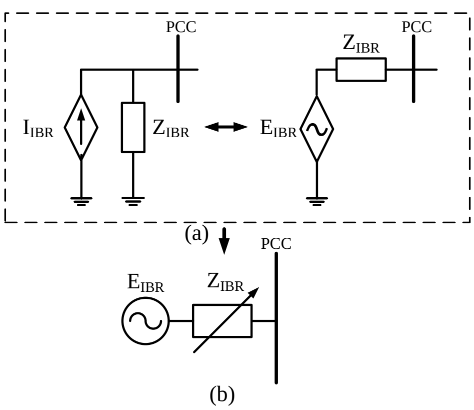

Fig. 1. Equivalent model of IBR: (a) with variable source and impedance, (b) with fixed voltage source and variable impedance.

two-bus system connecting an IBR to the grid is depicted in Fig. 2. A fault is assumed to occur at a distance of x pu from bus M with a fault resistance R_F. The grid is modeled using a voltage source E_G and an equivalent impedance Z_G.

The corresponding sequence networks for different asymmetrical faults are shown in Fig. 3, where Z_{RP} represents

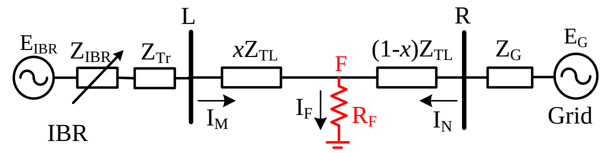

Fig. 2. Two bus equivalent system integrating an IBR to grid.

the combined impedance of Z_{IBR} and transformer impedance Z_{Tr}. Subscripts '0', '1', and '2' denote zero, positive, and negative sequence components respectively, and R_{ph} represents the inter-phase arcing resistance. The negative sequence network of the renewable plant is modeled as an open circuit, considering the inverter to be controlled in synchronous reference frame with feed-forward control. The zero-sequence network is constructed considering a dYg transformer configuration. Sequence quantities are computed using phase-A as the reference for AG, BC, and BCG faults. Relations for fault

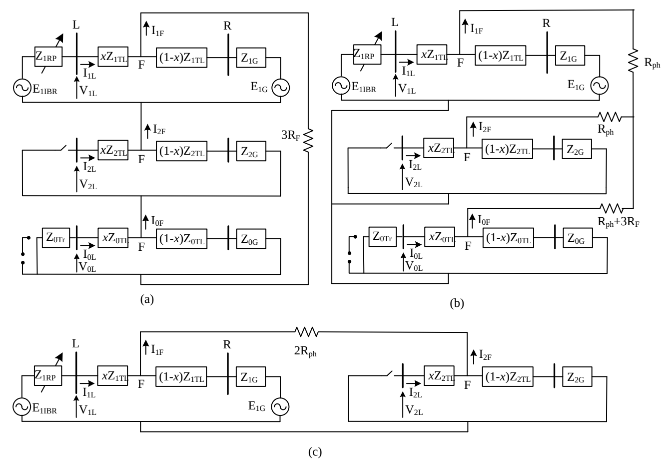

Fig. 3. Sequence network for (a) AG, (b) BC and (c) BCG faults.

type classification are formulated below by analyzing sequence networks for different types of faults.

1) For AG faults:: As in Fig. 3(a), the positive and negative sequence currents in faulted path for AG faults are equal. Superscript represents the reference phase for sequence component calculation.

$$I_{1F}^a = I_{2F}^a \tag{1}$$

Therefore, the relations between I_{1F} and I_{2F} for AG faults are expressed, as in (2).

$$\angle \left(I_{2F}^a / I_{1F}^a \right) = \quad 0 \tag{2}$$

2) For BC faults:: I_{1F} and I_{2F} are in phase opposition for BC faults (refer Fig. 3(b)).

$$I_{1F}^a = -I_{2F}^a \tag{3}$$

The relations between I_{1F} and I_{2F} for BC faults are presented in (4).

$$\angle \left(I_{2F}^a / I_{1F}^a \right) = \quad \pi \tag{4}$$

979-8-3315-8138-1

3) For BCG faults:: As in Fig. 3(c), the sequence currents in the faulted path for BCG faults are related by (5).

$$I^a_{1F} = -(I^a_{2F} + I^a_{0F}) \tag{5}$$

Homogeneity between negative and zero sequence impedance angles in a transmission network results in I^a_{2F} and I^a_{0F} to be in same phase. Thus, I^a_{1F} and I^a_{2F} are considered almost in phase opposition, similar to BC faults and the relation derived in (4) remain valid even with ground involvement.

Sequence networks for any LG, LL and LLG fault remain same as in Fig. 3, only the reference phase for calculating sequence components changes. Phase-B is considered as the reference for BG, CA, and CAG faults; and phase-C for CG, AB, and ABG faults. Relations in (2) and (4) can be transformed for other fault types following (6), where $\alpha = e^{j\frac{2\pi}{3}}$ [15].

$$I^a_{1F} = I^b_{1F}/\alpha^2 = I^c_{1F}/\alpha \quad and \quad I^a_{2F} = I^b_{2F}/\alpha = I^c_{2F}/\alpha^2 \tag{6}$$

Following the consistency of the relations obtained in (2) and (4) for any system conditions, the fault type classification zones are presented in Fig. 4 [15].

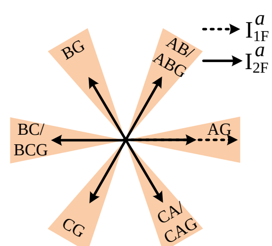

Fig. 4. System independent fault zones

B. Design of the virtual impedance-based phase modifier

Pure-fault positive and negative sequence networks for the system in Fig. 2 are shown in Fig. 5 (a) and (b).

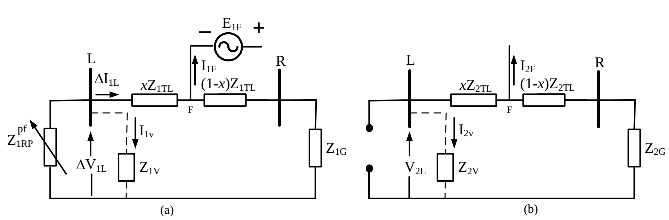

Fig. 5. Pure-fault (a) positive and (b) negative sequence network for the system in Fig. 2

Applying current division principle in Fig. 5(a), pure-fault positive sequence current at bus L (ΔI_{1L}) is obtained in (7).

$$\Delta I_{1L} = I_{1F} \times \frac{(1-x)Z_{1TL} + Z_{1G}}{Z^{pf}_{1RP} + Z_{1TL} + Z_{1G}} \tag{7}$$

Multiplying both sides with $(-Z^{pf}_{1RP})$, (7) is rewritten in (8).

$$(-Z^{pf}_{1RP})\Delta I_{1L} = I_{1F} \times \frac{(1-x)Z_{1TL} + Z_{1G}}{Z^{pf}_{1RP} + Z_{1TL} + Z_{1G}} \times (-Z^{pf}_{1RP}) \tag{8}$$

Considering grid impedance to be homogeneous to the line impedance, Z_{1G} can be expressed in terms of Z_{1TL} with a real-valued multiplier K. Applying this (8) is simplified in (9).

$$\Delta V_{1L} = I_{1F} \times \frac{(1-x+K)Z_{1TL}}{Z^{pf}_{1RP} + Z_{1TL} + Z_{1G}} \times (-Z^{pf}_{1RP}) \tag{9}$$

With some rearrangement of variables, (9) is rewritten in (10).

$$(1-x+K)I_{1F} = \frac{(-\Delta V_{1L})}{\dfrac{Z_{1TL} \cdot Z^{pf}_{1RP}}{Z^{pf}_{1RP} + Z_{1TL} + Z_{1G}}} \tag{10}$$

$(1-x+K)$ being a positive real value, it can be concluded from (10) that a current (I_{1v}) associating a phase angle same to I_{1F} can be observed to flow through a virtual impedance (Z_{1V}) when connected across a voltage, ΔV_{1L} with reverse polarity (i.e. $-\Delta V_{1L}$). I_{1v} and Z_{1V} are presented in (11).

$$I_{1v} = (1-x+K)I_{1F} \quad \text{and} \quad Z_{1V} = \frac{Z_{1TL} \cdot Z^{pf}_{1RP}}{Z^{pf}_{1RP} + Z_{1TL} + Z_{1G}} \tag{11}$$

In order to obtain Z_{1V}, Z^{pf}_{1RP} is calculated by applying (12).

$$Z^{pf}_{1RP} = -\frac{\Delta V_{1L}}{\Delta I_{1L}} \tag{12}$$

Grid being dominated by conventional synchronous generators, the equivalent impedance of the grid is assumed to remain unchanged during initial period of faults with the situation just before the fault. Applying the Thevenin equivalent estimation approach available in [16], Z_{1G} can be determined using three consecutive voltage and current measurement sets at bus M, obtained at different instances during prefault and send the information to the relay bus before fault avoiding any time delay in decision.

Most of the IBRs being controlled in positive sequence reference frame with feedforward control do not generate any negative sequence current. There I_{2F} in Fig. 5(b) is fully contributed by grid and can be expressed as in (13).

$$I_{2F} = \frac{-V_{2F}}{(1-x)Z_{2TL} + Z_{1G}} = \frac{-V_{2L}}{(1-x+K)Z_{2TL}} \tag{13}$$

After a rearrangement, (13) is rewritten in (14).

$$(1-x+K)I_{2F} = \frac{-V_{2L}}{Z_{1TL}} \tag{14}$$

Similar to positive sequence, it can be concluded from (14) that a current (I_{2v}) associating a phase angle same to I_{2F} can be observed to flow through a virtual impedance (Z_{2V}) when connected across a voltage, V_{2L} with reverse polarity (i.e. $-V_{2L}$). I_{2v} and Z_{2V} are expressed in (15).

$$I_{2v} = (1-x+K)I_{2F} \quad \text{and} \quad Z_{2V} = Z_{1TL} \tag{15}$$

Note: If the IBR is controlled with dual-sequence controller and injects negative sequence current in the system, the virtual negative sequence impedance in such a case can be obtained in similar way as explained for positive sequence component.

979-8-3315-8138-1

C. Implementation of the proposed approach

The steps involved in implementing the proposed fault type classification technique is presented in Fig. 6. The equivalent positive-sequence grid impedance $Z1G$ is estimated using local voltage and current measurements under prefault conditions and is continuously updated until a fault is detected. Upon fault detection, the relay checks the negative sequence voltage and current components. If both quantities are found to be negligible, the relay concludes that all three phases are faulted. Otherwise, it calculates $\angle(I_{2v}/I_{1v})$ and compares with the zones as mention in Fig. 4 to identify the fault type.

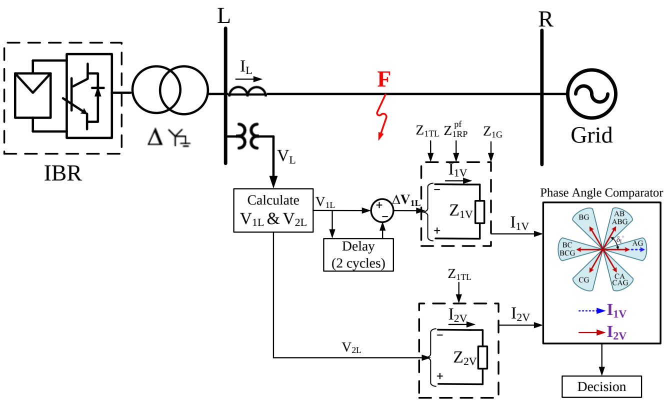

Fig. 6. Overview of the proposed fault type classification approach.

III. Results

Performance of the proposed phase selection method is evaluated on a 230 kV, 60 Hz, renewable integrated 9-bus system, as shown in Fig. 7. System simulations are performed in the PSCAD/EMTDC environment. Voltage and current phasors are extracted using a one-cycle discrete Fourier transform with a sampling rate of 3.84 kHz. A 200-MVA PV plant is interfaced to bus 3 through a grounded dYg transformer, and its inverter operates in the synchronous reference frame with feed-forward control near unity power factor. The proposed scheme is additionally evaluated by substituting the PV plant with Type-III and Type-IV wind farm models, tested individually.

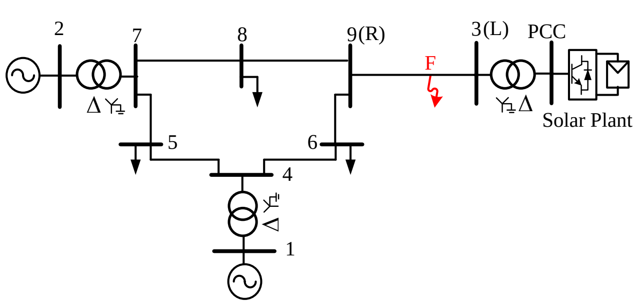

Fig. 7. Renewable integrated 9-bus test system.

A. Performance evaluation with comparative assessment

The response of the relay located at bus 3 in Fig. 7 is assessed for an AG fault applied at 5 s on line 3–9, at a distance of 0.25 pu from bus 3 with a fault resistance of 0.5Ω. As shown in Fig. 8, the conventional current-angle-based classifier [7] estimates $\delta_I^+ = -40^0$, which lies outside the decision region of the δ_I^+ comparator of Fig. 4, resulting in an incorrect fault-type decision. The voltage-based technique in [7] similarly misclassifies the event, yielding $\delta_V^+ = 28^0$, which also falls beyond the AG identification zone illustrated in Fig. 8. These observations highlight the limitations of both methods. In contrast, the proposed classifier computes $\delta_I^+ = -0.9^0$ following the procedure in Fig. 6, correctly identifying the AG fault.

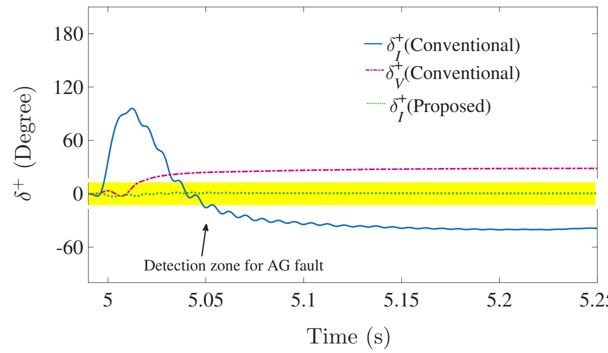

Fig. 8. Relative angles for AG fault.

B. Performance evaluation with different types of IBRs

IBRs exhibit diverse control strategies and converter configurations depending on the generation technology, leading to notable variations in their fault-current contributions. The proposed method sets the value of virtual impedance-based phase modifier accordingly, that enables accurate fault-type identification under varying IBR conditions. This capability is demonstrated using the relay at bus 3 for faults on line 3–9. The PV plant at bus 3 is successively replaced by a Type-III and then a Type-IV wind farm. As illustrated in Fig. 9, the conventional current-angle-based classifier yields δ_I^+ values of -168^0, 58.5^0, and 116.4^0 for an AG fault in the presence of the PV source, Type-III wind farm, and Type-IV wind farm, respectively—demonstrating how differing IBR characteristics can cause misclassification. In contrast, the proposed approach consistently places the computed relative angles within their correct decision regions and accurately identifies the AG fault, confirming its adaptability across diverse source types and control schemes.

IV. Hardware Prototype Implementation

A laboratory prototype incorporating the proposed fault-classification technique has been developed, as illustrated in Fig. 10. Various fault scenarios are generated on the PSCAD-based test system, and the corresponding voltage and current waveforms are transferred to MATLAB. The proposed logic is executed on an Arduino UNO R4 Wi-Fi board interfaced with MATLAB using the Arduino GFX and SSD1306 libraries.

979-8-3315-8138-1

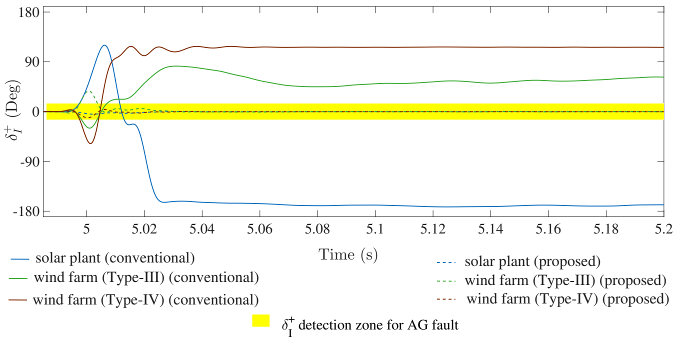

Fig. 9. Performance evaluation of proposed method for different types of CIRP with comparative assessment.

Fault indications are provided through dedicated LEDs for each phase and ground, while an SSD1306 OLED display presents the identified fault type along with the computed relative angle used in the decision process. The prototype demonstrates reliable and consistent performance.

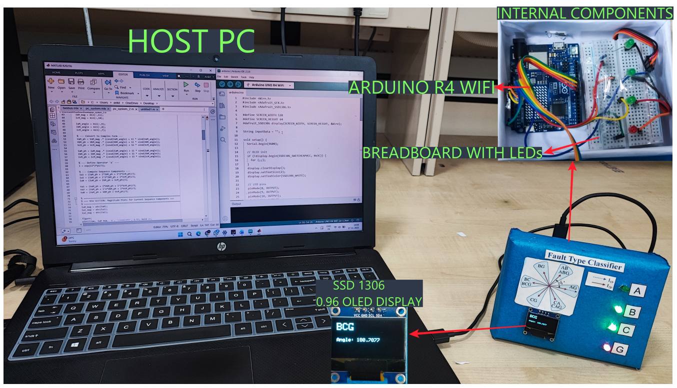

Fig. 10. Experimental setup with hardware prototype.

V. Conclusion

Control actions within IBRs create substantial non-uniformity in their fault-current contributions, which diminishes the reliability of conventional fault-classification methods that rely solely on local measurements. This work introduces an adaptive, local measurement-based design of a virtual impedance–based phase modifier framework that enables accurate fault-type identification for lines connected to IBRs. The method exhibits consistent performance across a wide range of fault scenarios with different IBRs, highlighting its robustness. Comparative analyses confirm that the proposed scheme achieves higher classification accuracy than existing approaches. The successful operation of the hardware prototype further supports the feasibility of implementing the method in real-time protection systems.

References

[1] 'Renewables Integration in India' (NITI Ayog, International Energy Agency, 2021).

[2] "IEEE Standard for Interconnection and Interoperability of Inverter-Based Resources (IBRs) Interconnecting with Associated Transmission Electric Power Systems," IEEE Std 2800-2022 , vol., no., pp.1-180, 22 April 2022.

[3] Paladhi, S., Pradhan, A. K.: 'Adaptive distance protection for lines connecting converter-interfaced renewable plants', IEEE J. Emerg. Sel. Topics Power Electr., 2021, 9, (6), pp. 7088–7098.

[4] Jia, K., Yang, Z., Fang, Y., Bi, T., Sumner, M.: 'Influence of inverter-interfaced renewable energy generators on directional relay and an improved scheme', IEEE Trans. Power Electr., 2019, 34, (12), pp. 11843–11855.

[5] Chowdhury, A., Paladhi, S., Pradhan, A. K.: 'Adaptive unit protection for lines connecting large solar plants using incremental current ratio', IEEE Syst. J., 2022, 16, (2), pp. 3272–3283.

[6] Paladhi, S., Pradhan, A. K.: 'Adaptive fault type classification for transmission network connecting converter-interfaced renewable plants', IEEE Syst. J., 2021, 15, (3), pp. 4025–4036.

[7] Kasztenny, B., Campbell, B., Mazereeuw, J., 'Phase selection for single-pole tripping - weak infeed conditions and cross country faults' (GE Power Management, 2000), pp. 1–19.

[8] Roberts, J. B., Schweitzer III, E. O.: 'Fault identification system for use in protective relays for power transmission lines'. US Patent 5,515,227, May 1996.

[9] Reddy, M. J., Mohanta, D. K.: 'Adaptive-neuro-fuzzy inference system approach for transmission line fault classification and location incorporating effects of power swings', IET Gen., Trans., Dist., 2008, 2, (2), pp. 235–244.

[10] Jena, M. K., Samantaray, S. R.: 'Data-mining-Bbased intelligent differential relaying for transmission lines including UPFC and wind farms', IEEE Trans. Neural Net. Learn. Syst., 2016, 27, (1), pp. 8–17.

[11] Azzouz, M. A., Hooshyar, A.: 'Dual current control of inverter-interfaced renewable energy sources for precise phase selection', IEEE Trans. Smart Grid, 2019, 10, (5), pp. 5092–5102.

[12] Song, G., Wang, C., Wang, T., Kheshti, M., Kang. X.: 'A phase selection method for wind power integration system using phase voltage waveform correlation', IEEE Trans. Power Del., 2017, 32, (2), pp. 740–748.

[13] Paladhi, S., Pradhan, A. K.: 'Adaptive zone-1 setting following structural and operational changes in power system', IEEE Trans. Power Del., 2018, 33, (2), pp. 560–569.

[14] Swain, K. B., Mahato, S. S., Cherukuri, M.: 'Expeditious situational awareness-based transmission line fault classification and prediction using synchronized phasor measurements', IEEE Access, 2019, 7, pp. 168187–168200.

[15] Paladhi, S., Hong, Q., Booth, C., 'Adaptive faulted phase selection for lines connecting converter-based sources' (Proc. 11th International Conference on Renewable Power Generation, 2022), pp. 228–232.

[16] Paladhi, S., Pradhan, A. K.: 'Resilient protection scheme preserving system integrity during stressed condition', IET Gen., Trans., Dist., 2019, 13, (14), pp. 3188–3194.

979-8-3315-8138-1